Frequency locking of meandering spiral waves in cardiac tissue

Bradley J. Roth
Department of Physics and Astronomy, Vanderbilt University, Nashville, Tennessee 37235
(Received 9 January 1998)

The influence of anisotropy on spiral waves meandering in a sheet of cardiac tissue is studied numerically. The FitzHugh-Nagumo model represents the tissue excitability, and the bidomain model characterizes the passive electrical properties. The anisotropy ratios in the intracellular and extracellular spaces are unequal. This condition does not induce meandering or destabilize spiral waves; however, it imposes fourfold symmetry onto the meander path and causes frequency locking of the rotation and meander frequencies when the meander path has nearly fourfold symmetry. [S1063-651X(98)50204-8]

PACS number(s): 87.90+y

Spiral waves of electrical activity underlie many cardiac arrhythmias [1]. Several authors have studied the dynamics of spiral waves in excitable media [2–5]. For example, Winfree studied the meandering of spiral waves using a two-dimensional reaction-diffusion model with FitzHugh-Nagumo kinetics [3]. As he varied the parameters in his model, the tip of his spiral wave traced a variety of paths, from a circle to a regular isogon (quasiperiodic meandering) to a chaotic-appearing contour. Barkley also studied meandering, and showed that there is no frequency locking within the quasiperiodic regime [4].

The heart has unique electrical properties, resulting in behavior that is not present in other excitable media. These properties arise from the anisotropy of cardiac tissue, and in particular from the different degrees of anisotropy in the intracellular and extracellular spaces (unequal anisotropy ratios) [6]. Winfree's and Barkley's models did not take into account unequal anisotropy ratios. In this Rapid Communication, I extend their calculations to include the effect of the bidomain model, which accounts for unequal anisotropy ratios [7]. My goal is to determine if the fourfold symmetry inherent in the bidomain model results in frequency locking during spiral wave meandering.

The bidomain model is a two- or three-dimensional cable model that is often used to represent the electrical properties of cardiac tissue [6,8,9]. It consists of two coupled partial differential equations [9]:

$$\frac{\partial \Phi_m}{\partial T} = \frac{1}{\varepsilon} f(\Phi_m, v) + \frac{\partial^2 \Phi_m}{\partial X^2} + \frac{\partial^2 \Phi_m}{\partial Y^2} + \frac{\alpha e}{1+\alpha(1-e)} \frac{\partial^2 \Psi}{\partial X^2}, \tag{1}$$

$$\left(2+\alpha+\frac{1}{\alpha}\right)\frac{\partial^2 \Psi}{\partial X^2} + \left(2+\alpha(1-e)+\frac{1}{\alpha(1-e)}\right)\frac{\partial^2 \Psi}{\partial Y^2} = e\left(1+\frac{1}{\alpha(1-e)}\right)\frac{\partial^2 \Phi_m}{\partial Y^2}. \tag{2}$$

Equation (1) is a reaction-diffusion equation for the transmembrane potential Φ_m. The last term in Eq. (1) is unique to the bidomain model; it represents the influence of unequal anisotropy ratios on Φ_m. I define the parameter e as one minus the ratio of conductivity ratios in the extracellular and intracellular spaces, $e = 1 - [(g_{ex}/g_{ey})/(g_{ix}/g_{iy})]$, where g_{ix} is the intracellular conductivity in the x direction, g_{ey} is the extracellular conductivity in the y direction, etc. [9]. When these two spaces have the same anisotropy ($g_{ex}/g_{ey} = g_{ix}/g_{iy}$), e equals zero. In that case, Eqs. (1) and (2) decouple and Eq. (1) reduces to that used by Winfree [3]. In ventricular muscle, e is approximately 0.75 [10], and the case of $e = 0.9$ exaggerates the influence of unequal anisotropy ratios. The parameter α is equal to g_{ix}/g_{ex} [9]; in my simulations, $\alpha = 1$ [10]. Equation (2) governs the auxiliary potential Ψ, which is a linear combination of the intracellular and extracellular potentials [9]. For $e = 0$, Eq. (2) reduces to Laplace's equation. Determining Ψ requires solving a boundary-value problem at every moment. X, Y, and T are dimensionless space and time variables; X is parallel to the myocardial fibers, and Y is perpendicular to them. The spatial variables are scaled such that for $e = 0$ the tissue is isotropic.

The FitzHugh-Nagumo model [3] specifies the function $f(\Phi_m, v)$ in Eq. (1), which governs the nonlinear membrane current. The variable v controls the recovery of the action potential.

$$f(\Phi_m, v) = \Phi_m - \frac{\Phi_m^3}{3} - v, \tag{3}$$

$$\frac{\partial v}{\partial T} = \varepsilon(\Phi_m + \beta - \gamma v). \tag{4}$$

Equations (3) and (4) contain three parameters: ε, indicating the ratio of recovery rate to excitation rate; β, relating to excitability; and γ, equal to $\frac{1}{2}$ in all of my calculations [3]. I consider values of ε from 0.1 to 0.3, and values of β greater than $\frac{2}{3}$ (an excitable medium incapable of local spontaneous oscillations).

TABLE I. Computational parameters.

ε	0.3 and 0.2	0.1
ΔX, ΔY	0.222	0.150
ΔT	0.0080	0.003 33
N_X, N_Y	271	401

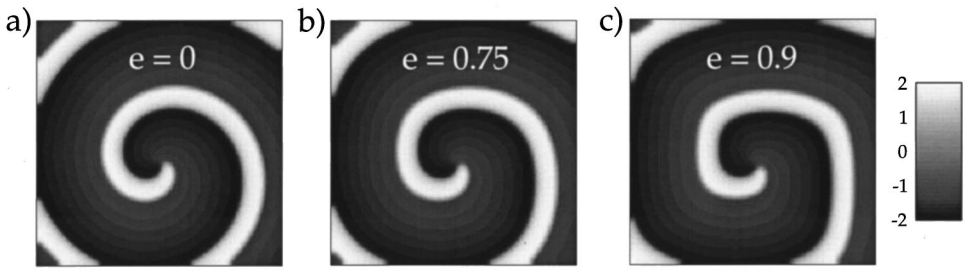

FIG. 1. The transmembrane potential $\Phi_m(X,Y)$ of a spiral wave; $T=200$, $\varepsilon=0.2$, $\beta=0.8$; (a) $e=0$, (b) $e=0.75$, and (c) $e=0.9$. Each panel is 60×60 space units.

Equations (1), (2), and (4) are coupled. I solve Eqs. (1) and (4) using an explicit finite-difference algorithm, and Eq. (2) at each time using overrelaxation [11]. The space and time steps (ΔX, ΔY, ΔT) depend on e (Table I). The overrelaxation terminates when the residual is less than 10^{-3}. The number of nodes in the X and Y directions (N_X, N_Y) are selected so that the tissue extends 60 space units in each direction (Table I). The edges of the tissue are insulated ($\partial\Phi_m/\partial n=\partial\Psi/\partial n=0$). Initial conditions are selected so that a single spiral wave develops. Typical simulations last for 800 time units. I ignore $T=0-200$, eliminating transients. For $T>200$, the spiral wave tip follows a path that is independent of the initial conditions.

The X coordinate of a meandering spiral wave tip, $X_{\rm tip}(T)$, is approximately the sum of two periodic motions: the spiral rotation, with frequency f_1, and the tip meandering, with frequency f_2 [5]. To calculate f_1 and f_2, I compute the Fourier transform of $X_{\rm tip}(T)$ and determine the frequency of the two primary peaks in the spectrum. Long computations are needed to determine the frequency accurately, so I limited these calculations to $\varepsilon=0.2$, $\Delta X=\Delta Y=0.3333$, $N_X=N_Y=181$, and $\Delta T=0.016\,66$. I ran these simulations for at least 1600, and up to 6000, time units.

Figure 1(a) shows a fully developed spiral wave; $T=200$, $e=0$, $\varepsilon=0.2$, and $\beta=0.8$. I define the period of a spiral wave τ_0 as the time between consecutive excitations at $X=Y=0$ (bottom left corner). If the spiral wave meanders, I average the last six periods. In Fig. 1(a), $\tau_0=12.8$. Increasing e gives a squarish shape of the spiral [Figs. 1(b) and 1(c)], but has a negligible effect on τ_0. Figure 2(a) shows $\Psi(X,Y)$ for $e=0.75$. Figure 2(b) shows $\partial^2\Psi/\partial X^2$, which is proportional to the last term in Eq. (1). $\partial^2\Psi/\partial X^2$ is largest where the wave front is propagating 45° to the fiber direction, and it has a depolarizing influence at the leading edge of the wave front.

My primary interest is in the path of the spiral wave tip. I define the tip as the location where $|\nabla\Phi_m\times\nabla v|$ is maximum [12]. The tip follows a nearly circular path for some values of β and ε, but for other values it meanders [3]. Figure 3(a) shows a circular tip path for equal anisotropy ratios; $\varepsilon=0.3$, $\beta=0.8$ ($\tau_0=48.4$). For unequal anisotropy ratios, the tip follows a simple but not circular path [Figs. 3(b) and 3(c)]. The period is almost independent of e ($e=0.75$, $\tau_0=48.7$; $e=0.9$, $\tau_0=49.6$). Varying e while fixing ε and β neither induces nor suppresses meandering.

Figure 4(a) shows that for $e=0$, $\varepsilon=0.2$, $\beta=0.8$, the spiral wave tip meanders along a path resembling a four-petal flower (Fig. 4, inset). The orientation of the flower precesses with a period of about 200 time units. For $e=0.75$ [Fig. 4(b)], the petals of the flower favor particular directions in space. For $e=0.9$ [Fig. 4(c)], the spiral and meander frequencies are entrained. The meander path is a closed quatrefoil, except for a slow, linear drift.

An even more interesting meander path occurs for a three-petal flower. Figure 5(a) shows the meander path for $e=0$, $\varepsilon=0.1$, $\beta=1$ ($\tau_0=18.4$). The path is nearly a trefoil (Fig. 5, inset). Figure 5(b) shows the path for $e=0.75$. The three-petal flower does an intricate dance that imposes a fourfold symmetry onto the meander path. The tip meanders through a convoluted path for $e=0.9$ [Fig. 5(c)], roaming over a large area (≈300 space units^2). The flower sometimes drifts almost linearly and at other times makes hairpin turns. The entire pattern repeats itself approximately every 2000 time units.

Previous studies of spiral wave meander indicated that f_1 and f_2 do not entrain [4]. In other words, as a parameter (such as β in the FitzHugh-Nagumo model) varies, f_1/f_2 changes continuously and does not favor simple integer ratios. However, Fig. 4(c) suggests that the bidomain model introduces frequency locking. Figure 6 shows f_1/f_2 as a function of β. The ratio changes smoothly for $e=0$, but for $e=0.75$ and $e=0.9$ it locks at $f_1/f_2=3$ over a range of values for β. A ratio of 3:1 corresponds to a closed, four-petal flower. Other simple frequency ratios, such as 4:1, do not show frequency locking. I find evidence of frequency locking for a ratio of 7:1 (eight-petal flower), although entrainment occurs over a much narrower range of β than for the 3:1 case. The bidomain model has little influence on the rotational frequency, f_1; the meander frequency f_2 is responsible for frequency locking. When there is no frequency locking, the bidomain model may still influence the tip path.

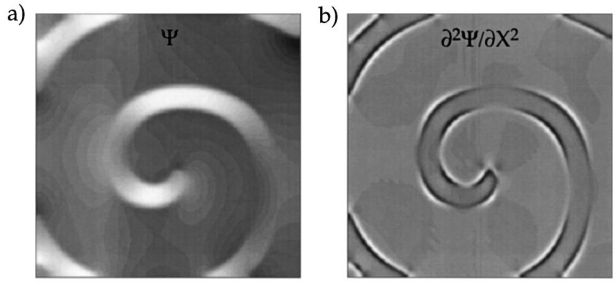

FIG. 2. (a) The auxiliary potential $\Psi(X,Y)$, and (b) $\partial^2\Psi/\partial X^2$ of a spiral wave; $T=200$, $\varepsilon=0.2$, $\beta=0.8$, and $e=0.75$. In (a), Ψ varies from 1.5 (white) to -1.5 (black). In (b), $\partial^2\Psi/\partial X^2$ varies from 0.5 (white) to -0.5 (black). Each panel is 60×60 space units.

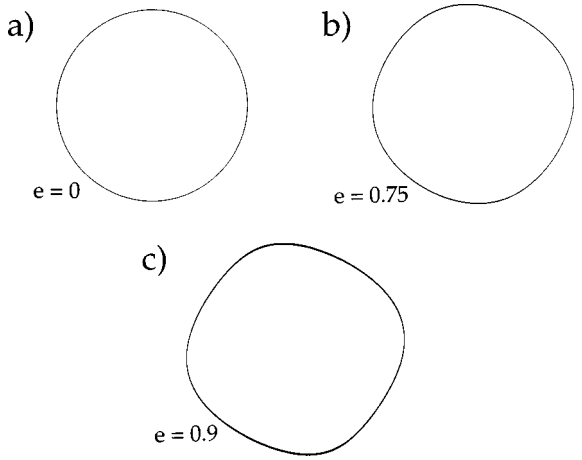

FIG. 3. Path of the tip of the spiral wave; $T=200-800$, $\varepsilon=0.3$, $\beta=0.8$, and (a) $e=0$, (b) $e=0.75$, and (c) $e=0.9$. The bar represents one space unit.

In particular, additional frequency components may contribute to the tip motion.

My results for $e=0$ are consistent with Winfree's report [3]. The inclusion of unequal anisotropy ratios in these calculations does not induce or suppress meandering, cause the meandering to become chaotic, or break up the spiral wave into fibrillation. However, the condition of unequal anisotropy ratios influences the meander path of the tip of the spiral wave and induces frequency locking, even for parameters corresponding to normal ventricular muscle ($e=0.75$).

Many phenomena associated with unequal anisotropy ratios contain a fourfold symmetry [13]. The condition of unequal anisotropy ratios imposes a similar fourfold symmetry on the meander patterns in Figs. 3–5. When the meander path is a nearly fourfold-symmetric isogon [Fig. 4(a)], the unequal anisotropy ratios entrain the meander path and cause frequency locking [Fig. 4(c)]. When the symmetry of the meander path is nearly threefold [Fig. 5(a)], unequal anisotropy ratios cause the tip of the spiral wave to undergo a rather complicated dance that imposes a fourfold symmetry when viewed over long times.

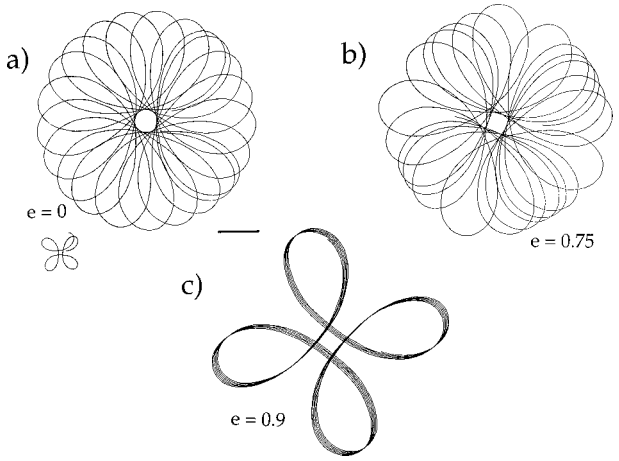

FIG. 4. Path of the tip of the spiral wave; $T=200-425$, $\varepsilon=0.2$, $\beta=0.8$, and (a) $e=0$, (b) $e=0.75$, and (c) $e=0.9$. The inset shows $e=0$ for $T=200-245$. The bar represents one space unit.

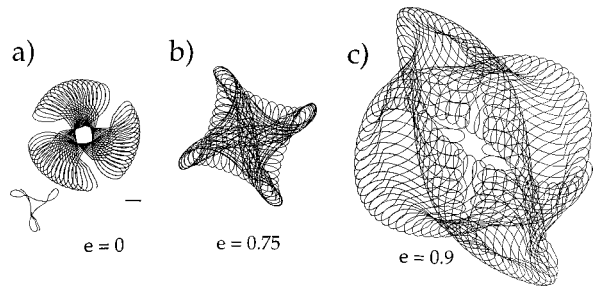

FIG. 5. Path of the tip of the spiral wave; $\varepsilon=0.1$, $\beta=1.0$, and (a) $e=0$, (b) $e=0.75$, and (c) $e=0.9$. The inset shows $e=0$ for $T=200-245$. The bar represents one space unit.

Insight into the origin of the fourfold symmetry can be found in a perturbation analysis of the bidomain equations in the parameter e [9]. A second-order contribution results in a fourfold symmetric pattern of Φ_m leading a closed, circular wave front [9]. A similar effect is present in Fig. 2(b), where

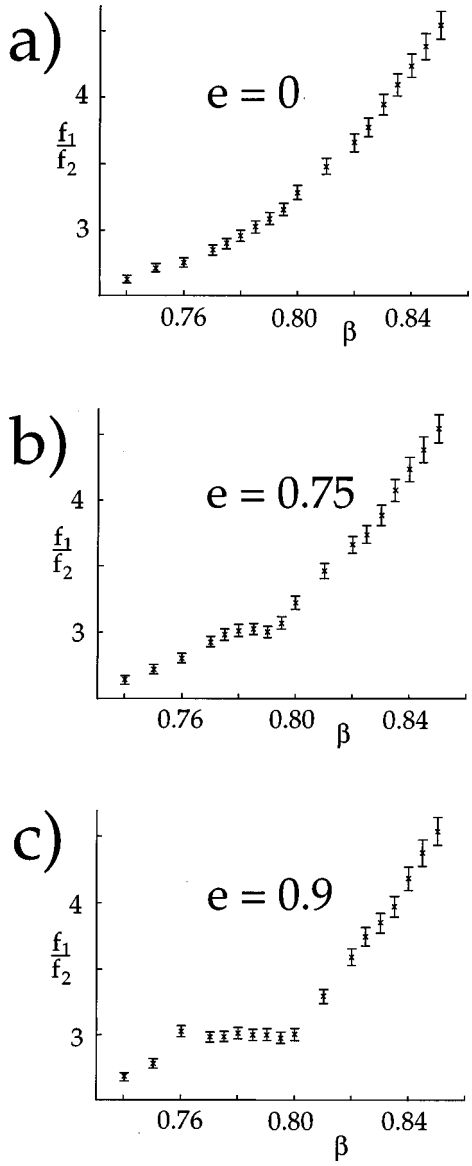

FIG. 6. The ratio of rotational frequency f_1 to meander frequency f_2 as a function of β; $\varepsilon=0.2$, (a) $e=0$, (b) $e=0.75$, and (c) $e=0.9$. Frequency locking occurs at $f_1/f_2=3$.

the additional source term is largest 45° from the fiber direction, and is nearly zero parallel to and perpendicular to the fibers. Although this bidomain effect is second order in e and therefore small, it can have significant impact because propagation at the spiral wave tip is compromised by wave-front curvature and incomplete recovery.

Barkley [4] analyzed spiral wave dynamics using a bifurcation analysis. He found that one of the primary eigenvalues of a spiral wave is associated with rotational symmetry. My results imply that the bidomain model breaks the rotational symmetry, and should therefore modify the eigenvalue spectrum.

Keener [14] studied propagation in cardiac tissue using a model that, like mine, does not preserve rotational symmetry. His model, however, postulates a discrete medium, with the degree of ''discreteness'' different in each direction. My model, on the other hand, is continuous, and the rotational symmetry is broken by the properties of the bidomain model with unequal anisotropy ratios.

This research was supported by the Whitaker Foundation and the College of Arts & Sciences, Vanderbilt University. I thank Barry Bowman for his careful editing of the manuscript. Discussions with Rubin Aliev and Art Winfree improved the manuscript.

[1] A. T. Winfree, in *Cardiac Electrophysiology, From Cell to Bedside*, 2nd ed., edited by D. P. Zipes and J. Jalife (Saunders, Philadelphia, 1995), pp. 379–389.

[2] V. S. Zykov, Biophysics **5**, 940 (1986); A. Karma, Phys. Rev. Lett. **65**, 2824 (1990); V. G. Fast and A. M. Pertsov, Biophysics **35**, 489 (1990); A. Karma, Phys. Rev. Lett. **66**, 2274 (1991); **71**, 1103 (1993).

[3] A. T. Winfree, Chaos **1**, 303 (1991).

[4] D. Barkley, Phys. Rev. A **42**, 2489 (1990); D. Barkley, Phys. Rev. Lett. **68**, 2090 (1992); D. Barkley, *Chemical Waves and Patterns*, edited by R. Kapral and K. Showalter (Kluwer, Dordrecht, 1995), pp. 163–189.

[5] G. S. Skinner and H. L. Swinney, Physica D **48**, 1 (1991); G. Li, Q. Ouyang, V. Petrov, and H. L. Swinney, Phys. Rev. Lett. **77**, 2105 (1996).

[6] B. J. Roth, J. Math. Biol. **30**, 633 (1992).

[7] B. J. Roth, Bull. Am. Phys. Soc. **42**, 1808 (1997); in *Proceedings of the 1997 International Conference on Mathematical Models in Medical and Health Sciences* (Vanderbilt University Press, Nashville, 1998); in *Cardiac Electrophysiology, From Cell to Bedside*, 3rd ed., edited by D. P. Zipes and J. Jalife (Saunders, Philadelphia, in press).

[8] C. S. Henriquez, Crit. Rev. Biomed. Eng. **21**, 1 (1993).

[9] B. J. Roth, Phys. Rev. E **55**, 1819 (1997).

[10] B. J. Roth, IEEE Trans. Biomed. Eng. **44**, 326 (1997).

[11] B. J. Roth, J. Cardiovasc. Electrophysiol. **7**, 722 (1996).

[12] W. Jahnke, W. E. Skaggs, and A. T. Winfree, J. Phys. Chem. **93**, 740 (1989).

[13] N. G. Sepulveda and J. P. Wikswo, Jr., Biophys. J. **51**, 557 (1987); N. G. Sepulveda, B. J. Roth, and J. P. Wikswo, Jr., *ibid*. **55**, 987 (1989); J. M. Saypol and B. J. Roth, J. Cardiovasc. Electrophysiol. **3**, 558 (1992).

[14] J. P. Keener, J. Math. Biol. **26**, 41 (1988).